Guiding the Experimental Search: Computational Discovery of Palladium Jewelry Alloys with Enhanced Hardness

Jacqueline Corbitt

A senior thesis submitted to the faculty of
Brigham Young University
in partial fulfillment of the requirements for the degree of

Bachelor of Science

Dr. Gus Hart, Advisor

Department of Physics and Astronomy

Brigham Young University

June 2011

ABSTRACT

Guiding the Experimental Search: Computational Discovery of Palladium Jewelry Alloys with Enhanced Hardness

Jacqueline Corbitt
Department of Physics and Astronomy
Bachelor of Science

Stable structures were determined in three binary metallic systems–palladium/copper, palladium/magnesium, and palladium/niobium–using computational programs based on Schrödinger's equation and basic thermodynamics. These programs determined the formation enthalpies of each combinatorially-possible structure, ignoring the effects of temperature. This investigation only looked at structures up to 12 atoms large. Monte Carlo methods were used to determine the approximate phase transition temperature—the temperature at which it will become thermodynamically stable for the atoms to order rather than be randomly placed—for several of the anticipated stable structures. Structures with high transition temperatures are more likely to be experimentally feasible. Information about the predicted stable structures and their respective transition temperatures will guide the work of experimentalists who develop these alloys.

Keywords: computational, materials science, palladium, alloys, thermodynamics, cluster expansion, ground state search, first principles, VASP

ACKNOWLEDGMENTS

Thank you to my family for always supporting me, and thank you to my research advisor, Dr. Gus Hart.

Contents

Chapter 1

Introduction

In this chapter, we discuss the motivation for this research and previous findings which have influenced our study. Historically, alloys have been used to make materials harder, and this is important for metal alloys frequently used in jewelry in order to retain their shape. Recent calculations suggest that previously unobserved Pd-rich binary alloys may form in some systems. We have investigated three of these systems in this paper.

1.1 Background

Gold is an important element in the jewelry industry. However, in jewelry applications, one rarely uses gold in its pure form. Typically, gold jewelry is 14-18 karats (58.3%-75.0% gold by weight), and hardly ever 24 karats (100% gold). Why is this? Because pure gold is too soft to make sturdy jewelry. If the gold mixture used in gold jewelry was pure gold, the jewelry would bend, become misshapen very easily, and scratch. Jewelers know that if they mix other elements in with the gold they can make a gold alloy[1] which is harder than the original gold, and thus create jewelry which will keep its shape.

[1] An alloy is a mixture of two or more elements, at least one of which is a metal.

From the example of gold, we see that alloys can be harder than the original elements. We apply this principle to other elements, in this case, palladium (Pd). Jewelry is an important market for Pd. Over the last 10 years, 10% of the world's available Pd was used in jewelry. [2] Pd, like gold, is too soft to be used in jewelry, but we know from experimental work that alloying Pd with another element can increase its hardness. This increases Pd's suitability for jewelry application.

We look for new Pd-rich metallic alloys which can be used in jewelry applications by investigating the potential of Pd-rich mixtures to form crystal structures. Using computation, we can predict both the thermodynamic stability of these alloys and the approximate temperature at which these alloys will form. Experimentalists who develop Pd-rich alloys use these predictions to drastically narrow their search, since with these predictions they can look for just a few predicted structures, alloys, and concentrations, instead of investigating thousands of alloy possibilities.

An important constraint on Pd alloys suitable for jewelry application is the international jewelry hallmarking standards. These standards require that jewelry alloys be 95% Pd by weight to be classified as Pd jewelry. For example, in order to be "stamped" Pd jewelry, if we have one gram of a Pd alloy, at least 0.95 gram would be Pd and no more than 0.05 gram would be any other element. Most experimental Pd-X structures of the form Pd-X, where X is some other element, are not sufficiently rich in Pd to meet this jewelry standard. Our research focuses on predicting the stability of Pd-rich binary alloys which also satisfy this 95% requirement and thus could be candidates for use in jewelry.

1.2 History

Recent calculations and experiments suggest that unsuspected Pd-rich ordered phases[2] may form in several Pd binary alloys. [3] A phase with the prototype Pt_8Ti (Pearson symbol tI18 and space

[2]The terms *structure*, *configuration*, and *ordered phase* are interchangeable.

group I4/mmm, see Fig. 1.1), discovered in 1959, has been experimentally observed in several Pd-based systems, including Pd_8W, Pd_8V, and Pd_8Mo. [4] (*Prototype* refers to the system in which this crystal structure was first observed.) Because this structure has shown a tendency to be stable in some Pd systems (in addition to some Pt and Ni systems, which are in the same family as Pd), we use it as an indicator to test the completeness of the set of experimentally-verified ground states in several Pd binary systems. We can calculate the formation enthalpy of this structure and compare it to the formation enthalpies of experimentally-verified ground states. If the formation enthalpy of the Pd_8X structure is comparatively lower than the ground states, then this indicates that the experimentalists may not have observed all energetically stable structures, and there is cause for investigation to determine the stable structures so that experimentalists can begin to develop them.

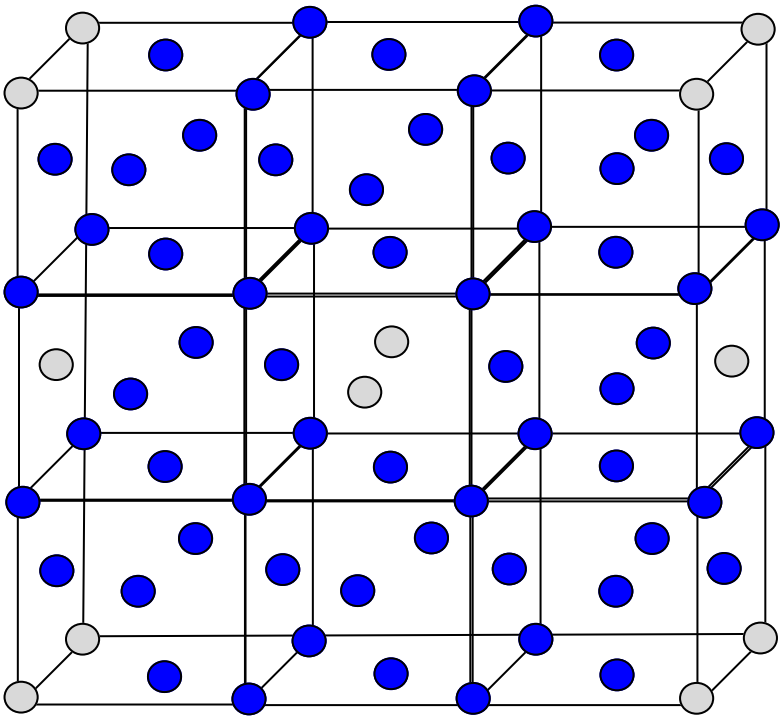

Figure 1.1 This figure shows the Pt_8Ti structure. Light gray circles represent the placement of Ti atoms, and dark blue circles represent the placement of Pt atoms.

Our primary resource to determine which structures have already been seen in experiment is

phase diagrams for each of our systems. Reading phase diagrams is a complicated task which we will not describe in detail in this paper. However, an example is included in Fig. 1.2. It suffices to say that the phase diagrams graphically represent the Pd concentration and temperature range of observed ground states in each system, and, when known, list the exact atomic structure of these ground states.

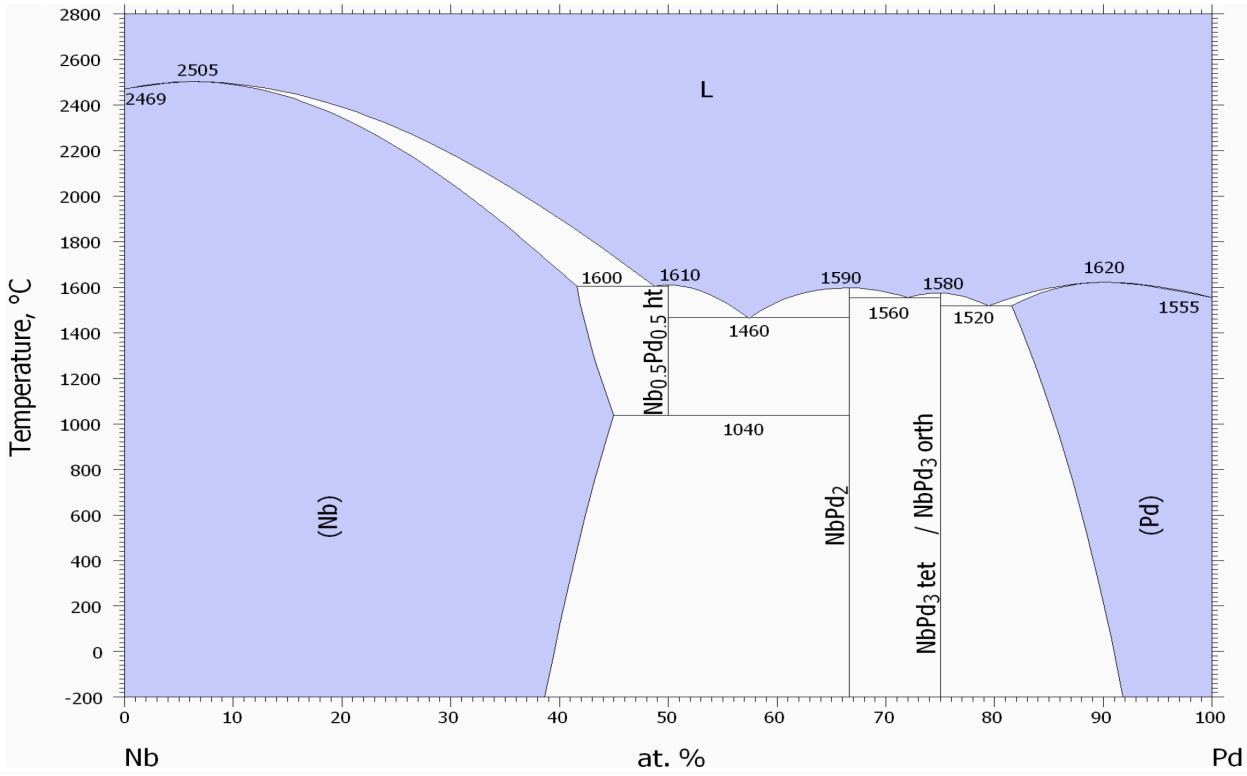

Figure 1.2 This is an example of a phase diagram. This is a published Pd-Nb phase diagram incorporating existing data. The vertical axis represents temperature and the horizontal axis represents increasing concentration of Pd in the mixture. [1]

Of the three systems I chose to investigate—palladium-copper (Pd-Cu), palladium-magnesium (Pd-Mg), and palladium-niobium (Pd-Nb)—very few Pd-rich structures have been observed. In fact, the phase diagrams showed that no Pd-rich structures have been experimentally observed in either the Pd-Cu or Pd-Mg systems, but two Pd-rich structures have been found in the Pd-Nb system. For more information on the specific structures, see Chap. 3, which includes tables

of the structures seen in experiment vs. the structures we computationally predicted.[3] These systems were chosen in part because they were some of the first Pd systems that we determined had the possibility for new structures. [5] In this paper I have focused solely on the possible Pd-rich configurations for each of these systems.

[3]When we refer to comparing our structures to the Pd-rich side of the phase diagram, we mean that we have compared the Pd-rich configurations we have predicted to what has been experimentally observed in the phase diagram.

Chapter 2

Computational Methods

In this chapter, we discuss the methods used to determine the stable structures in Pd-Cu, Pd-Mg, and Pd-Nb.

2.1 General Method

When elements bond, energy is either released or absorbed in the process of forming the new compound. For example, when hydrogen and oxygen combine to make water, the reaction gives off heat. This indicates that energy has been released in the process, and since energy was released in bonding, energy would be needed to break it apart. This indicates that the molecule is unlikely to break apart spontaneously and consequently is stable. This description is a slight simplification of the more complex chemistry, but it is the key principle for our investigation.

The energy released or absorbed in a combination reaction, such as in the example of water above, is known as the *formation enthalpy*. When energy is released in binding, as in hydrogen and oxygen binding to make water, this formation enthalpy is negative and the molecule is stable.

Since we use a computational approach, we have the ability to investigate the energies of all possible structures in a system. We use an algorithm (developed by Hart et.al. [6, 7]) which enu-

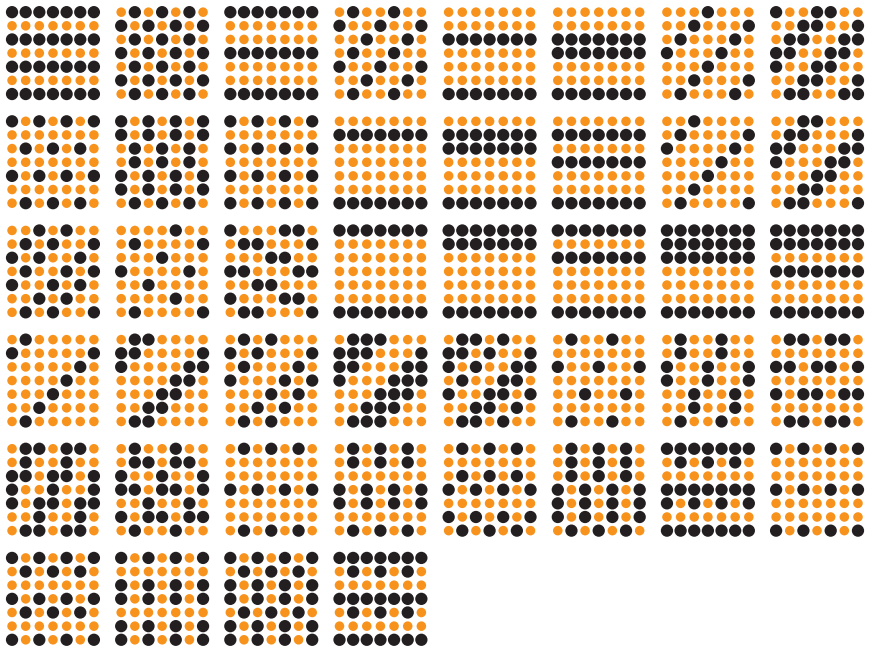

Figure 2.1 This figure shows several possible cell patterns on a 7×7 grid.

merates all unique crystal structures up to a given cell size. Since we have the tools to calculate the structures' respective energies, we can thus calculate the energy of any structure.

A structure refers to a unique repeating unit of atoms, also known as a cell. In Fig. 2.1, we see several different types of cells on a 7×7 grid.[1] This grid is referred to as a lattice, with each atom position known as a *lattice site*. We can see in the leftmost cell that there is a two-atom pattern, with one yellow and one black atom each. A small box could be drawn around the two leftmost atoms on the top row as shown in Fig. 2.2. This small box could be repeated in any direction to continue drawing the same structure. This small box is known as the *unit cell*, or a "tile" that can be periodically repeated to create the entire crystal. The other cells in Fig. 2.1 have different patterns and also have different unit cells (see Fig. 2.2). The cell size is determined by how many atoms are present in the unit cell, since this is the smallest possible unit of the structure.

Note: In our 2D example, the unit cell is a parallelogram which is defined by two vectors.

[1] This two-dimensional model is a simplification from our three-dimensional problem.

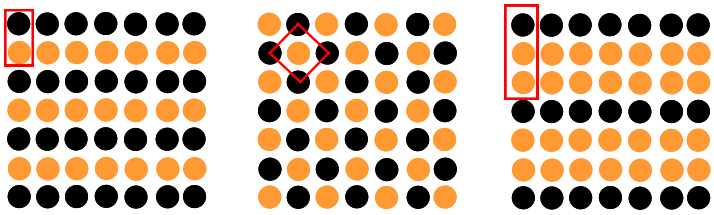

Figure 2.2 This figure shows the unit cell for a selected few cell patterns.

(We can see this when we examine Fig. 2.2; the vectors in these examples are two sides of the defined parallelogram which are not parallel to each other). In three dimensions, the unit cell is a parallelepiped and is defined by three vectors, rather than two.

In our approach, we calculate the formation enthalpy for 70-100 structures in each of our Pd-X systems—Pd-Cu, Pd-Mg, and Pd-Nb.[2] (In this paper, we will use the terms *energy* and *formational enthalpy* interchangeably.) These energies are calculated using a program called VASP (see Sec. 2.2). All of the formation enthalpies we calculated for possible structures in this system were negative, but since some enthalpies were more negative than others, the structures which correspond with the most negative formation enthalpies are the stable structures. These thermodynamically stable structures are *ground states*. We give the input of the structures and the corresponding energies to a cluster expansion program (Sec. 2.3). The cluster expansion is a fit, where the atomic arrangement is the independent variable and the corresponding energy is the dependent variable. The cluster expansion can quickly calculate the energies of other structures which were not part of the original input set. We used cross-validation scores to check the goodness of the fit. We use this tool to predict the energies of other atomic arrangements without using VASP.

[2] I looked at structures which were made up of 12 atoms or less [8], since in metallic systems, most ordered phases have a unit cell with 12 atoms or fewer. [9]

Once the energies of the structures have been predicted, we construct a *convex hull* (see Fig. 2.3) to determine which concentrations will be stable. The idea is that a mixture of elements will form the structure or structures which have the lowest possible formation enthalpy. Sometimes the structure at that concentration with the lowest energy is *not* stable, however, because a mixture of two different structures of different concentrations would have a lower overall formation enthalpy than the structure of that concentration. Thus, there is no ground state at this concentration.

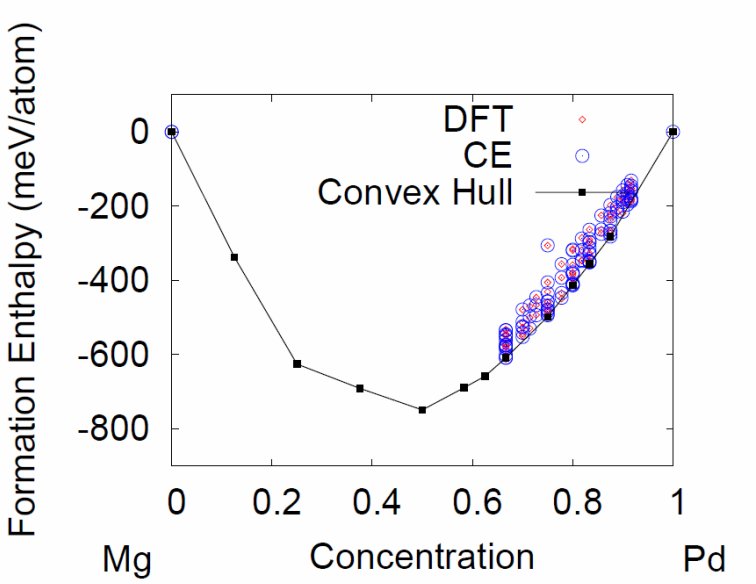

Figure 2.3 Here we see an example of a convex hull. The DFT and CE points represent energies calculated by VASP and by the cluster expansion, respectively. The points on the convex hull represent structures which will be stable at the indicated concentrations. See Fig. 3.2 for a more thorough explanation of the specific data represented.

Examine Fig. 2.3. The red diamonds represent energy calculations by VASP, and the blue circles represent the energy calculations for these structures using the cluster expansion. Each input structure is represented by both a red diamond and a blue circle; when the red diamond

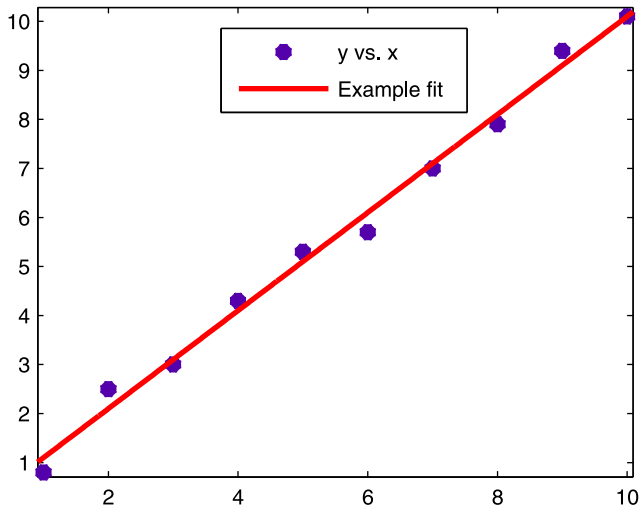

Figure 2.4 Just like a line through a data set will not match all the points exactly, neither will a cluster expansion perfectly match the energies calculated by VASP.

and blue circle are close together, this means that the energies calculated by VASP and by the cluster expansion for a given structure match closely. (See Fig. 2.4 for the explanation as to why the energies will not match perfectly.) The black line in Fig. 2.3 indicates the convex hull, and the black squares show the ground states. We can tell the concentration of the ground states by looking at the horizontal axis, which represents the atomic ratio of Pd to the whole cell.

As mentioned, ground states occur at only a few concentrations. Examine the case of Pd concentration $x = 78\%$ Pd. Although there are structures represented at this concentration, the energies of these structures are above the convex hull, so a mixture of two structures, the most stable 75% Pd structure and the most stable 80% Pd structure, would be more energetically favorable than any structure at exactly $x = 78\%$ Pd. So, in an experiment, if a mixture were to be made of 78% Pd and 22% Cu, the mixture would separate into the most stable 75% and 80% Pd structures. The concentration of the mixture would remain at $x = 78\%$ Pd, but neither structure would have concentration $x = 78\%$ Pd.

The transition temperature is the highest temperature at which the structure begins to form. It

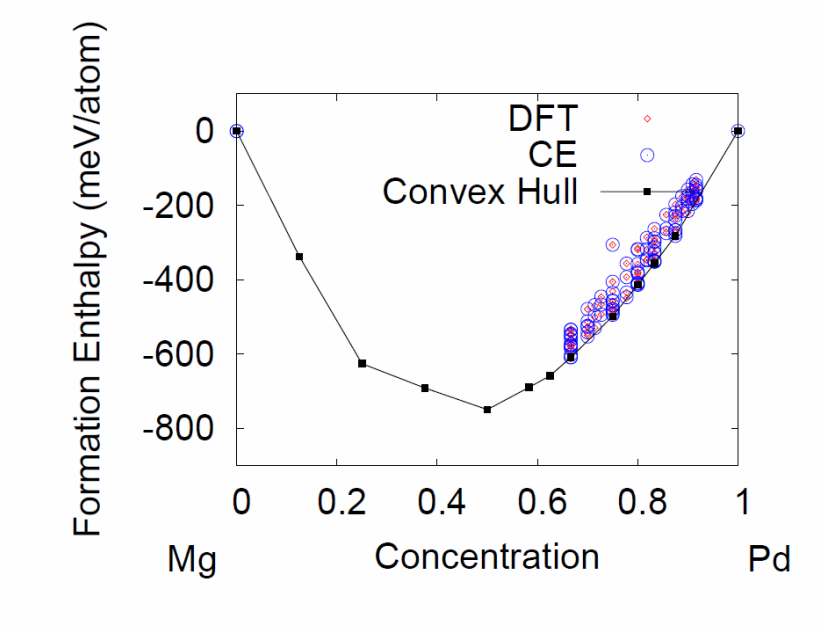

Figure 2.5 This figure, also used to demonstrate a convex hull, is an example of determining the ground states in a system. The red diamonds represent VASP calculations and the blue circles represent cluster expansion calculations. The convex hull is represented by a black line, and each black square represents a stable structure, or ground state. The vertical axis shows the formation enthalpy for each structure. Each structure is calculated twice, once by VASP and once by cluster expansion, and the closer these two points are together, the closer VASP and the cluster expansion agree with each other. Individual structures are not labeled.

is determined by the equation

$$F = U - TS \tag{2.1}$$

where F is the free energy, U is the internal energy of the system, T is the temperature of the system in K, and S is the entropy of the system. The system is the most stable when F is minimized. The transition temperature is defined as the temperature at which $\mathrm{F_{disordered}} = \mathrm{F_{ordered}}$. Above the transition temperature, F is minimized by maximizing entropy because $\mathrm{F_{disordered}} < \mathrm{F_{ordered}}$. This is achieved when lattice sites are occupied randomly. Below the transition temperature, F is

minimized by making U small. This is achieved by the atoms forming an ordered, stable state, which decreases the energy of the system.

If the temperature is below room temperature (about 298 K), the probability the atoms will change position becomes small, even if changing their final position would lead to a more stable arrangement. This is due to the energy barrier, or activation energy, of moving the atoms. In order to move to the more energetically favorable conditions, the atoms would need to temporarily move to less energetically-favorable positions. This temporary move requires energy that the atoms are statistically unlikely to have below room temperature. Therefore, if the transition temperature is below room temperature, the structure takes so long to form that it is impractical to wait long enough for it to happen. Thus, this calculation may rule out some structures for experimental work. We can predict the transition temperature for each ground state using Monte Carlo methods (explained in Sec. 2.4). Thus, experimentalists will not attempt to develop structures for which the predicted transition temperature is too low, but will rather focus on structures which are more likely to form in experiment.

2.2 First Principles Calculations

Schrödinger's equation provides the basis for our calculations, since it is the fundamental equation describing electron interactions. We use a computer program called Vienna Ab-Initio Simulation Package (VASP) that conceptually uses Schrödinger's equation to predict interactions between the atoms of a structure. [10, 11]

VASP is based on density functional theory (DFT), which reduces many-body electron interactions to simpler calculations by using an equation analogous to the wave functions of Schrödinger's equation. VASP uses a theory based on electron density rather than many-body wave functions. This avoids calculating a multibody wave function for the system while still providing highly ac-

curate energies. However, while DFT is more efficient than the full many-body solution, it is still computationally expensive. Depending on the structure, VASP can take days to calculate the energy of one structure. There are over ten thousand possible structures for cell sizes up to 12 atoms, and so solely relying on VASP for these calculations would be practically impossible. (As a reference, calculating the energies for every structure individually could take several months to a year. The cluster expansion method (Sec. 2.3), which uses relatively few input energies, runs for less than a day to create a fit, and takes less than 10 seconds to map the fit to all other energies.) Instead, we calculate only a few energies using this method and then use the cluster expansion to find good approximations for the formation enthalpies of the other structures.

2.3 Cluster Expansion

A cluster expansion is a fit between the given atomic structures and their (respective) formation enthalpies. We feed the cluster expansion program the configurations for dozens of structures and the corresponding formation enthalpies (calculated using VASP), and the cluster expansion algorithm calculates a fit to match these parameters. The cluster expansion can be applied to all enumerated structures, predicting energies for structures not calculated by VASP. [8]

The cluster expansion, although quick, is initially not as accurate as VASP. The early cluster expansion fits will predict certain structures to be ground states, but, due to a small input set, these predictions are not very reliable. We improve the cluster expansion by calculating the energies of the predicted ground states in VASP and then adding these structures and their VASP-calculated energies to the input set and making an improved fit. [8] We continue this cycle of calculating predicted ground states in VASP, running the cluster expansion, and comparing the cluster expansion energies for predicted ground states to the VASP-calculated energies for these structures for several iterations. [8] Eventually, the cluster expansion will match VASP calculations closely and will be

consistent with stable structures calculated by VASP. At this point we decide that the ground states of the system have been found.

The cluster expansion is a fit which describes the relationship between the structure (the independent variable) and the formation enthalpy (the dependent variable). This is akin to being given three (x,y) points and being asked to determine a quadratic equation which runs through all of these points. The quadratic equation would be the "fit" for these three points.

The cluster expansion, however, is more difficult to calculate. Instead of (x,y) points, we are given a structure with a corresponding energy, which is more complex due to more fitting parameters.[3] Additionally, instead of only three (x,y) points, we have 70-100 input structures and energies. Because we have more data points than degrees of freedom, we say that the cluster expansion is overdetermined.

To explain the concept of being overdetermined, we return to the quadratic example. Three points can be fit by a quadratic. Adding any more points to that data set would overdetermine the set. This is true because a quadratic has three parameters which vary in the equation:

$$y = ax^2 + bx + c \tag{2.2}$$

where a, b, and c are all variables which can be varied to make the final equation, or final fit. Thus, we see if we have three data points, the three variables can be determined exactly. However, if a fourth point was not exactly on the parabola determined by the first three points, the quadratic would need to be adjusted to come close to the fourth point, and it would no longer perfectly fit all the data. This is why we cannot expect the cluster expansion and VASP energies to match perfectly. Rather, we try to minimize the error between the fit and VASP data through successive iterations. Essentially, this is a least-squares fitting process.

Once the cluster expansion and VASP energy calculations match closely, the thermodynami-

[3] In our cluster expansion model, we set the number of variables which can be adjusted (like the a, b, c of the quadratic) to 20. Additional terms are insignificant.

cally stable structures can be determined through use of a convex hull. (See Sec. 2.1.) We have discovered that some concentrations have many structures with energies within 10% of each other, making it difficult to determine the actual structure of the ground state. However, this fact does not hinder development of the alloy. Experimentalists look for alloys to form at given concentrations because they have more direct control over that factor. Therefore, in their work, information about stable concentrations is more useful than specific structures.

2.4 Monte Carlo Methods

The energies calculated in VASP and in the cluster expansion have all been calculated ignoring effects of temperature, so effectively we have calculated these energies at $T = 0\,\mathrm{K}$. Using Monte Carlo methods, we look for a transition temperature (refer to the end of Sec. 2.1 of the predicted ground states in order to determine which ground states are more experimentally feasible.

At high temperatures, atoms are randomly distributed on the lattice sites (Sec. 2.1) and randomly diffuse from site to site. This is a *solid solution*. Below the transition temperature, however, the energetic stability from ordering overcomes the entropy gain of remaining disordered. Below the transition temperature, the atoms begin to preferentially diffuse to lower energy sites. Instead of random distribution, the atoms begin to be correlated. However, if the transition temperature is *too* low, the atoms do not have enough energy to change position, even if it is energetically favorable to do so. We do not face this challenge computationally, but it is a concern for experimentalists. Thus, determining the transition temperature is important for their work.

We use Monte Carlo (MC) methods to predict a transition temperature for each ground state. [8] MC methods approximate the thermodynamics of each structure by exchanging two atoms randomly within a large simulation cell. If the switch is energetically favorable, an algorithm known as the Metropolis Algorithm determines whether the switch will be kept: the likelihood of

keeping the switch is dependent on the temperature of the system and is determined by $e^{-\Delta E/(k_B T)}$. This models the thermodynamics of the system as temperature varies. [12] In our case, the MC simulations used a cell of 8000 atoms.

The temperature in the MC simulation is moved down by steps. For every temperature step, the simulation will perform a user-specified number of *flips*, or two-atom switches, to simulate the atoms moving in the cell. The MC simulation represents temperature change by making atoms less likely to switch as the temperature decreases, since the likelihood of keeping the switch is $e^{-\Delta E/(k_B T)}$. It is seen in the calculation that over a short number of temperature steps, the energy of the large cell suddenly decreases drastically (as demonstrated in Fig. 2.6), indicating the transition temperature of the configuration.

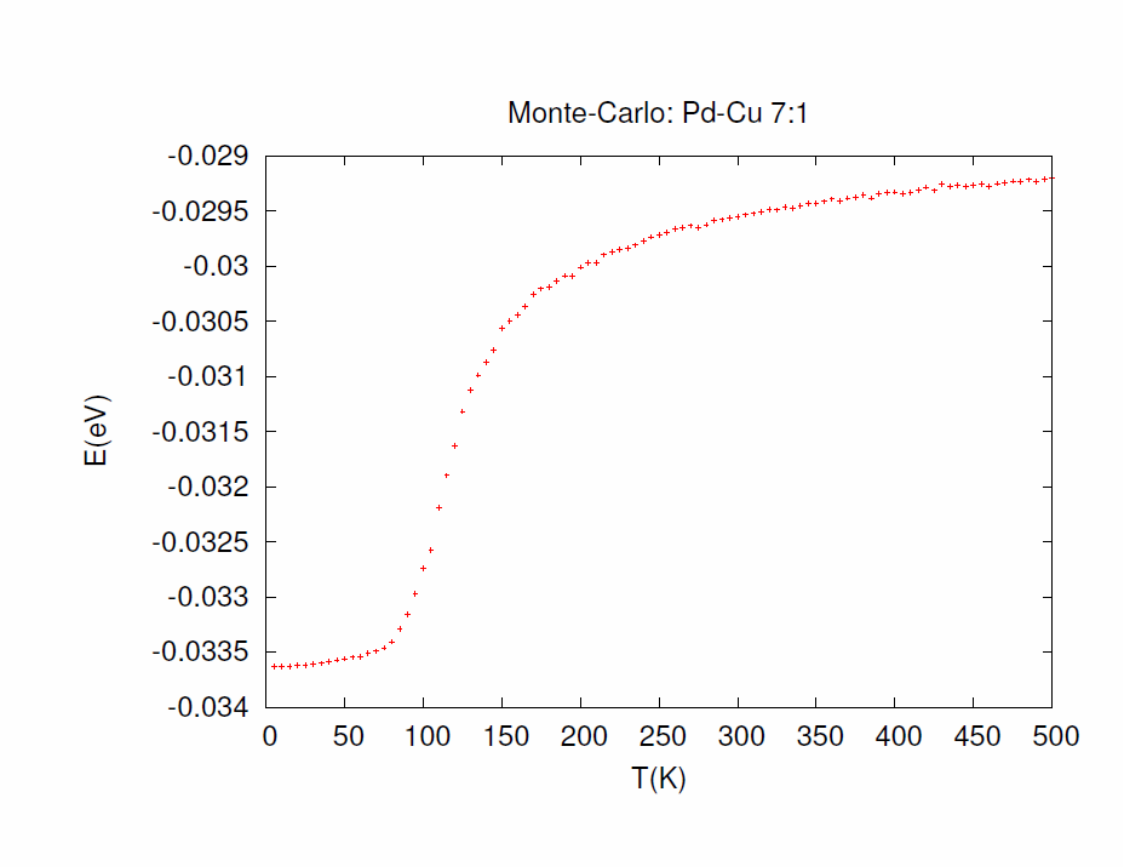

Figure 2.6 An example of determining the transition temperature for a structure. This figure shows the transition temperature for the structure with the stoichiometry 7 Pd to 1 Cu (92.1% Pd). The horizontal axis measures temperature in Kelvin and the vertical axis measures energy in eV. The transition temperature is the approximate temperature at which the energy drops steeply, which in this case is 150 K.

Chapter 3

Results

In this section, we report our results by giving a table summarizing our results for each system. Each table which shows the comparison between structures recorded in a phase diagram (experimental data) vs. our computationally-predicted structures (listed in the tables as *first-principles results*). In many cases, we predicted a ground state where the phase diagram did not report any stable structures. Concentrations where experimental data did not show a ground state is reflected in the table with either *Pd-rich fcc solid solution* or *two-phase region* as appropriate. None of these structures have been searched for (besides the structures in Pd-Nb which have already been experimentally observed).

Additionally, in these tables we list prototypes for structures which have been observed in different systems. Some structures we predicted are named in the literature, and these names are listed in the table. Some structures we predicted have not been observed and so do not have common names, and these are indicated by "new structure". Since these structures are not in the literature, we include Appendix A which lists the lattice vectors and atomic basis of these structures.

3.1 Pd-Cu

The input for the cluster expansion for Pd-Cu was constructed from first-principles formation enthalpies for 85 structures. This cluster expansion had an average error of about 8%.[1] Each MC simulation used an 8000 atom cell ($20 \times 20 \times 20$) with 10^5 flips per temperature step.[2]

The experimental phase diagram reports only an fcc solid solution on the Pd-rich half of the phase diagram, indicating that no Pd-rich structures have been observed. The only ordered phases reported in this phase diagram are at 1:1 stoichiometry (i.e. an atomic ratio of 1 Pd atom to 1 Cu atom) or are Cu-rich, with more Cu atoms than Pd atoms in a unit cell.

In our cluster expansion searches, we found four stable Pd-rich structures not previously reported in the literature. Three of the structures have known prototypes, i.e. these structures have been seen before in other systems (see Table 3.1). However, MC simulations indicate that transition temperatures are likely to be extremely low—in this case below room temperature–meaning that these structures are unlikely to form (see Sec.2.4). We include them in this thesis for completeness, although they are unlikely to be of practical use.

3.2 Pd-Mg

The input for the cluster expansion for Pd-Mg was constructed from first-principles formation enthalpies for 98 structures. This cluster expansion had an average error of about 2%. Each MC simulation used an 8000 atom cell ($20 \times 20 \times 20$) with 10^6 flips per temperature step.

The experimental phase diagram for Pd-Mg reports five ordered phases. However, the most Pd-rich phase has a 1:1 ratio of Pd to Mg, so it is not very Pd-rich. Thus, all Pd-rich structures we predict are new.

[1] In this case and in the other systems, the average error is the best fit we were able to achieve.

[2] In this case and in the other systems, we adjusted the number of flips (through trial and error) in order to achieve the most clear results.

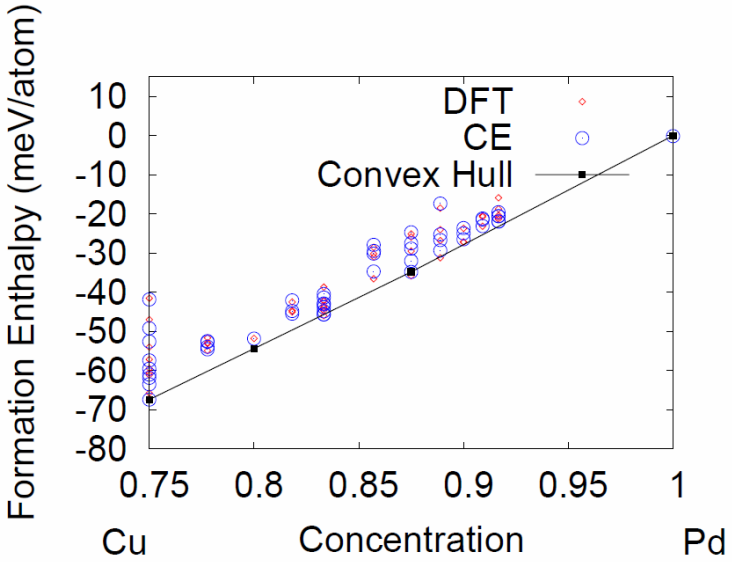

Figure 3.1 This figure shows the results of the Pd-Cu system. The key was described in Fig. 2.5.

The cluster expansion calculations show a number of Pd-rich stable phases, at stoichiometries 7:1, 5:1, 4:1, 3:1, and 2:1 (i.e. 7 Pd atoms to 1 Mg atom, etc). The first two of these listed ratios meet the hallmarking criteria for jewelry alloys, that is, they are 95% Pd by weight, since Mg is a light metal. However, with the exception of the 2:1 and 3:1 structures, the transition temperatures for these ordered phases are too low to be practical.

One note about the calculations: at 66.7% and 83.3%, the cluster expansion and first principles calculations disagreed on the specific structure which would be the most stable at these concentrations. However, the energy differences between the predicted structures is only a few meV/atom, less than 1% of the formation enthalpies, and so this difference is essentially insignificant. When experimentalists are looking for alloys, they will look for any structure forming at a concentration, and are less concerned about what the exact structure is. Therefore the small conflict between pre-

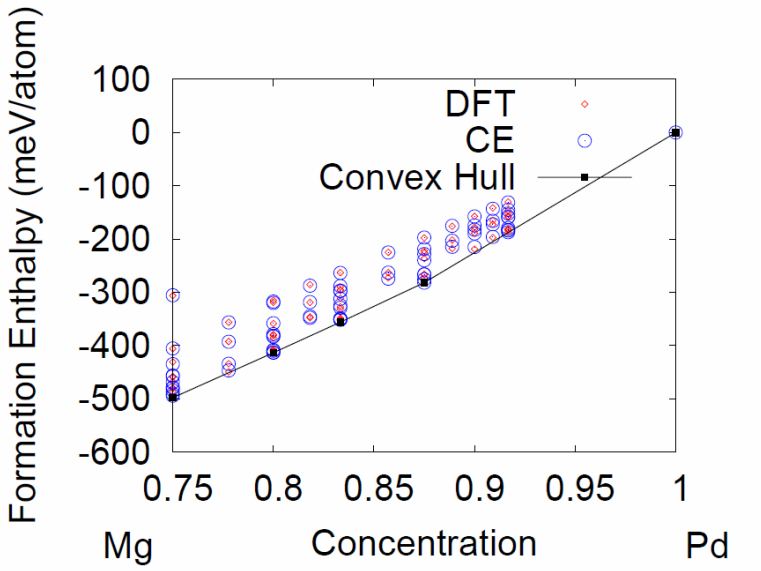

Figure 3.2 This figure shows the results of the Pd-Mg system. The key was described in 2.5. The key is the same for both systems.

Pd-Cu system		
Comparison of low temperature ground states		
% Pd	Experimental results [1, 13–16]	First principles results
66.7	*Pd-rich fcc solid solution*	$MoSi_2$ ($C11_b$) ($T_c \approx -100^\circ$ C)
75.0	*Pd-rich fcc solid solution*	$L1_2$ ($T_c \approx -150^\circ$ C)
80.0	*Pd-rich fcc solid solution*	New structure † ($T_c \approx -150^\circ$ C)
87.5	*Pd-rich fcc solid solution*	Ca_7Ge ($T_c \approx -150^\circ$ C)

Table 3.1 Experimental and first-principles comparison of ground states in the Pd-Cu system. (†) See Structure Tables in the Appendix for crystallographic description.

dicted structures is unimportant for our purposes. The table lists the structures predicted by cluster expansion calculations.

3.3 Pd-Nb

The input for the cluster expansion for Pd-Nb was constructed from first-principles formation enthalpies for 71 structures. This cluster expansion had an average error of about 2%. Each MC simulation used an 8000 atom cell ($20 \times 20 \times 20$) with 10^6 flips per temperature step for the 4:1 and 5:1 concentrations, and 8×10^4 flips per step for the 2:1, 3:1, and 8:1 concentrations.

Some of the structures we predicted for this system have already been experimentally observed. The Pd-Nb phase diagram reports the $MoPt_2$ prototype at 67% Pd and a combination of the $TiAl_3$ and $NbPd_3$ prototypes from about 72% to 78%. Thus, the cluster expansion results are consistent with experiment. There are two prototypes listed for the stoichiometry of 3:1; the $TiAl_3$ ($D0_{22}$) structure forms at a low temperature while the $NbPd_3$ structure forms at a high temperature. The *exact* transition temperatures of these structures are not indicated in the phase diagram, but finding either of these structures computationally is consistent with the phase diagram.

Pd-Mg system		
Comparison of low temperature ground states		
% Pd	Experimental results [1, 13, 17, 18]	First principles results
66.7	*two-phase region*	New structure † (T_c ≈1425° C)
75.0	*two-phase region*	$L1_2$ (T_c ≈475° C)
80.0	*Pd-rich fcc solid solution*	$D1_a$ (T_c ≈325° C)
83.3	*Pd-rich fcc solid solution*	New structure † (T_c ≈225° C)
87.5	*Pd-rich fcc solid solution*	$CuPt_7$ (T_c ≈175° C)

Table 3.2 Experimental and first principles comparison of ground states in the Pd-Mg system. (†) See Structure Tables in the Appendix for crystallographic description.

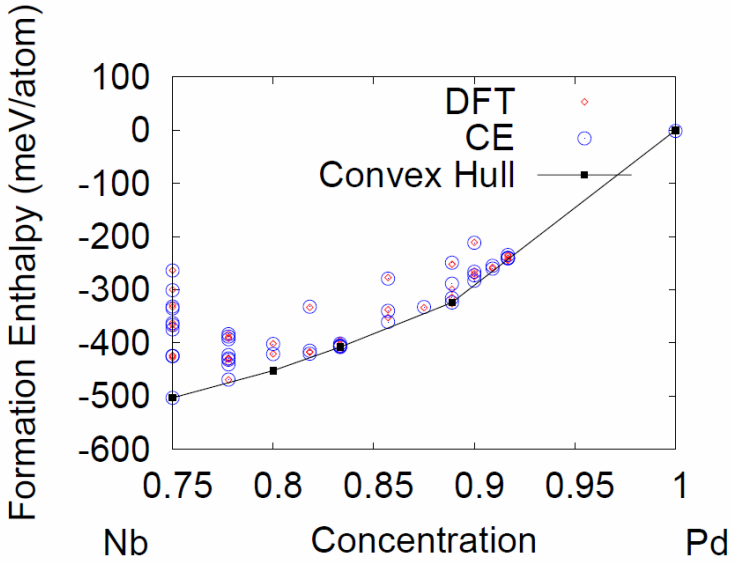

Figure 3.3 This figure shows the results of the Pd-Nb system. The key was described in 2.5. The key is the same for both systems.

The cluster expansion calculations show ground states at stoichiometries 8:1, 5:1, 4:1, 3:1, and 2:1 (i.e. 8 Pd to 1 Nb, 5 Pd to 1 Nb, etc). The 2:1 and 3:1 ground states are reported in the phase diagrams, but the other structures have not been observed in Pd-Nb. In order to meet the jewelry hallmarking standard, the concentration of Pd needs to be 95 atomic percent, so none of these structures independently met the criteria, but all predicted structures have a sufficiently high transition temperature to still form structures in a Pd-rich mixture.

3.4 Conclusion

A history of experimental results [22–35] which found Pd-rich ground states invited a large survey [3] that searched for the 8:1 phase (Pt_8Ti prototype) in other systems. Here we have examined three systems (Pd-Cu, Pd-Mg, Pd-Nb) in more detail, looking for this 8:1 phase and any other Pd-rich phases. In addition to first-principles-based ground state searches, we have also performed thermodynamic MC simulations to predict the transition temperatures for the predicted ground states.

We find several ground states that are not reported in the phase diagrams [1]. In each case, we find that either the 8:1 structure (prototype Pt_8Ti) or the 7:1 structure (prototype $CuPt_7$) is stable, as well as structures which have not been reported before in any system (so there are no known prototypes). Information for these structures is given in the Appendix A. In the case of Pd-Cu, the phases that have not been observed before experimentally are predicted to have very low transition temperatures. Our results indicate that currently unobserved ground states should be experimentally feasible in Pd-Mg and Pd-Nb.

These results direct experimentalists to the stable concentrations in the Pd-Mg and Pd-Nb systems, and also determines that Pd-rich structures in the Pd-Cu system are not good candidates for experimental investigation.

Pd-Nb system		
Comparison of low temperature ground states		
% Pd	Experimental results [1, 13, 19–21]	First principles results
66.7	$MoPt_2$	$MoPt_2$ ($T_c \approx 1225^\circ$ C)
75.0	$TiAl_3$ ($D0_{22}$) & $NbPd_3$	$D0_{22}$ ($T_c \approx 1275^\circ$ C)
80.0	*two-phase region*	$D1_a$
83.3	*Pd-rich fcc solid solution*	New structure †
88.9	*Pd-rich fcc solid solution*	Pt_8Ti ($T_c \approx 725^\circ$ C)

Table 3.3 Experimental and first principles comparison of ground states in the Pd-Nb system. (†) See Structure Tables in the Appendix for crystallographic description.

Appendix A

New Structures

Table A.1 Crystallographic data for other unrelaxed fcc-derived prototypes arising in our study.

Compound	Pd_8Cu_2	Pd_8Mg_4	$Pd_{10}Mg_2$	Pd_8Mg_4
Lattice	Orthorhombic	Orthorhombic	Monoclinic	Orthorhombic
Space group	Cmmm #65	Cmcm #63	P21/m #11	Pnma #62
Pearson Symbol	oS20	oS24	oP12	oP12
Primitive vect.				
$\mathbf{a}_1$/a	(0,0,-1)	(1,0,0)	(1,-1,-1)	(0,-1,0)
$\mathbf{a}_2$/a	(-1/2,5/2,0)	(1/2,3/2,0)	(-1/2,1/2,-1)	(1,0,-1)
$\mathbf{a}_3$/a	(1,0,0)	(0,0,2)	(1,1,0)	(3/2,0,3/2)
Atomic Positions				
A1	(0,0,0)	(0,0,0)	(0,0,0)	(0,0,0)
A2	(1/2,1/5,1/10)	(5/6,1/3,1/4)	(2/3,5/6,1/4)	(1/2,3/4,1/6)
A3	(0,2/5,1/5)	(2/3,2/3,1/2)	(1/3,2/3,1/2)	(0,1/2,1/3)
A4	(1/2,3/5,3/10)	(1/2,0,3/4)	(0,1/2,3/4)	(1/2,1/4,1/2)
A5	(0,4/5,2/5)	(1/3,1/3,0)	(2/3,1/3,0)	(0,0,2/3)
A6	(1/2,0,1/2)	(0,0,1/2)	(1/3,1/6,1/4)	(1/2,3/4,5/6)
A7	(0,1/5,3/5)	(2/3,2/3,0)	(0,0,1/2)	(1/2,1/4,1/6)
A8	(0,3/5,4/5)	(1/3,1/3,1/2)	(2/3,5/6,3/4)	(0,1/2,2/3)
A9	—	—	(1/3,2/3,0)	—
A10	—	—	(2/3,1/3,1/2)	—
B1	(1/2,2/5,7/10)	(1/6,2/3,1/4)	(0,1/2,1/4)	(0,1/2,0)
B2	(1/2,4/5,9/10)	(5/6,1/3,3/4)	(1/3,1/6,3/4)	(0,0,1/3)
B3	—	(1/2,0,1/4)	—	(1/2,3/4,1/2)
B4	—	(1/6,2/3,3/4)	—	(1/2,1/4,5/6)
Enum. label	1184	8196	7897	8054

Table A.2 Crystallographic data for other unrelaxed fcc-derived prototypes arising in our study.

Compound	Pd_5Mg_1	$Pd_{10}Nb_2$
Lattice	Orthorhombic	Orthorhombic
Space group	Cmmm #65	Pmmn #59
Pearson Symbol	oS12	oP12
Primitive vect.		
$\mathbf{a}_1$/a	(0,-1,0)	(0,-1,0)
$\mathbf{a}_2$/a	(1,0,0)	(1,0,-1)
$\mathbf{a}_3$/a	(-1/2,0,3/2)	(3/2,0,3/2)
Atomic Positions		
A1	(0,0,0)	(0,0,0)
A2	(1/2,1/6,1/3)	(1/2,3/4,1/6)
A3	(0,1/3,2/3)	(0,1/2,1/3)
A4	(1/2,1/2,0)	(1/2,1/4,1/2)
A5	(0,2/3,1/3)	(0,0,2/3)
A6	—	(1/2,3/4,5/6)
A7	—	(0,1/2,0)
A8	—	(1/2,1/4,1/6)
A9	—	(1/2,3/4,1/2)
A10	—	(0,1/2,2/3)
B1	(1/2,5/6,2/3)	(0,0,1/3)
B2	—	(1/2,1/4,5/6)
Enum. label	65	7922

Bibliography

[1] P. Villars, M. Berndt, K. Brandenburg, K. Cenzual, J. Daams, F. Hulliger, A. Prince, H. Putz, and S. Iwata, "The Pauling File, Binaries Edition," Journal of Alloys and Compounds **367,** 293–297 (2004).

[2] D. Jollie, "Platinium Uses," Technical report, Johnson Matthey (2009) .

[3] R. H. Taylor, S. Curtarolo, and G. L. W. Hart, "Predictions of the Pt_8Ti Phase in Unexpected Systems," Journal of the American Chemical Society **132,** 6851–6854 (2010).

[4] P. Pietrokowsky, Ph.D. thesis, .

[5] E. Gilmartin, Brigham Young University, Undergraduate thesis (unpublished).

[6] G. L. W. Hart and R. Forcade, "Generating derivative structures: Algorithm and applications," Phys. Rev. B **77,** 224115 (2008).

[7] G. L. W. Hart and R. Forcade, "Generating derivative structures from multilattices: Application to hcp alloys," Phys. Rev. B **80,** 014120 (2009).

[8] D. Lerch, O. Wieckhorst, G. L. W. Hart, R. W. Forcade, and S. Müller, "Constructing Cluster Expansions for Arbitrary Lattices from Minimal User Input," Model. Simul. Mater. Sci. Eng. **17,** 055003 (2009).

[9] S. Barthlein, E. Winning, G. L. Hart, and S. Muller, "Stability and instability of long-period superstructures in binary Cu-Pd alloys: A first principles study," Acta Materialia **57,** 1660 – 1665 (2009).

[10] G. Kresse and J. Furthmüller, "Efficient iterative schemes for ab initio total-energy calculations using a plane-wave basis set," Physical Review B **54,** 11169–11186 (1996).

[11] G. Kresse and J. Hafner, "Ab initio molecular dynamics for liquid metals," Physical Review B **47,** 558–561 (1993).

[12] N. Metropolis, A. W. Rosenbluth, M. N. Rosenbluth, A. H. Teller, and E. Teller, "Equation of State Calculations by Fast Computing Machines," Journal of Chemical Physics **21,** 1087–1092 (1953).

[13] *Binary Alloy Phase Diagrams*, T. Massalski, H. Okamoto, P. Subramanian, and L. Kacprzak, eds., (American Society for Metals, Materials Park, OH, 1990).

[14] A. Soutter, A. Colson, and J. Hertz, "Etude cristallographique des phases ordonnees a grande distance et particulierement des structures antiphases monoperiodiques et biperiodiques presentes dans les alliages binaires cuivre-palladium," Memoires Scientifiques de la Revue de Metallurgie **68,** 575–591 (1971).

[15] D. Fisher, D. Chisdes, and T. Flanagan, "Solution of Hydrogen in Palladium/Copper Alloys," Journal of Solid State Chemistry **20,** 149–158 (1977).

[16] M. Guymont and D. Gratias, "On the Stability of Periodically Antiphased Alloys," Physica Status Solidi A: Applied Research **36,** 329–334 (1976).

[17] E. Savitskii, V. Terekhova, and N. Birun, "Equilibrium Diagram of the Mg-Pd System," Russian Journal of Inorganic Chemistry **7,** 1228–1231 (1962).

[18] S. R. R. Ferro, "Ricerche sulle leghe dei metalli nobili con gli elementi piu elettropositivi," Atti della Accademia Nazionale dei Lincei, Classes di Scienze Fisiche, Matematiche e Naturali **29,** 70–73 (1960).

[19] A. K. E.M. Savitskii, V.V. Baron, "Equilibrium Diagram of the Niobium-Palladium System," Russian Journal of Inorganic Chemistry **6,** 1316–1317 (1961).

[20] K. Schubert, K. Frank, R. Gohle, A. Maldonado, H. Meissner, A. Raman, and W. Rossteutscher, "Einige Strukturdaten metallischer Phasen," Naturwissenschaften **50,** 542–543 (1963).

[21] B. Giessen, N. Grant, D. Parker, R. Manuszewski, and R. Waterstrat, "The Niobium (Columbium)-Palladium Constitution Diagram," Metallurgical Transactions, Section A: Physical Metallurgy and Materials Science **11,** 709–715 (1980).

[22] P. Pietrokowsky, "Novel ordered phase, Pt_8Ti," Nature **206,** 291 (1965).

[23] P. Krautwasser, S. Bhan, and K. Schubert, Z. Metallkde. **59,** 724–729 (1968).

[24] W. E. Quist, C. van der Wekken, R. Taggart, and D. H. Polonis, Trans. Met. Soc. AIME **245,** 345–349 (1969).

[25] J. M. Larson, R. Taggart, and D. H. Polonis, Metall. Trans. **1,** 485–489 (1970).

[26] H. A. Moreen, R. Taggart, and D. H. Polonis, J. Mater. Sci. **6,** 1425–1432 (1971).

[27] L. Weaver and A. J. Ardell, Scripta Metall. **14,** 765–768 (1980).

[28] A. J. Ardell and K. Janghorban, *Phase Transitions During Irradiation* (Applied Sci. Pub., London, 1982), pp. 291–329.

[29] D. Schryvers and S. Amelinckx, "Order-Disordered Phenomena in the Platinum Rich Part of the Pt-V Phase Diagram," Acta Metallurgica **34,** 43–54 (1986).

[30] D. Schryvers, J. V. Landuyt, and S. Amelinckx, "Electron Microscopy Study of a New Ordered Phase in the Platinum-Vanadium (8:1) System," Material Research Bulletin **18,** 1369–1374 (1983).

[31] J. Mayer and K. Urban, Phys. Stat. Sol.(a) **90,** 469–475 (1985).

[32] M. S. Mostafa and A. J. Ardell, Mater. Lett. **3,** 67–70 (1987).

[33] M. P. Nzula, C. I. . Lang, and D. J. H. Cockayne, J. All. Comp. **420,** 165–170 (2006).

[34] J. van dder Wekken, R. Taggart, and D. H. Polonis, "Short-Range Order and the Nucleation of Long-Range Order in Ni-Rich Nickel-Niobium Alloys," Metal Science Journal **5,** 219–223 (1971).

[35] J. Cheng and A. J. Ardell, "On the Stability of the ordered Pd_8V Phase in a Proton-Irradiated Pd-15at%V Alloy," Journal of the Less-Common Metals **141,** 45–53 (1988).

Index